Mon. Not. R. Astron. Soc. **000**, 1–10 (2005) Printed 4 February 2008 (MN LATEX style file v2.2)

Restrictions on parameters of sterile neutrino dark matter from observations of galaxy clusters.

A. Boyarsky[1,2,3], A. Neronov[4,5], O. Ruchayskiy[6], M. Shaposhnikov[2,1]
[1] *CERN, Theory department, Ch-1211 Geneve 23, Switzerland*
[2] *École Polytechnique Fédérale de Lausanne, Institute of Theoretical Physics, FSB/ITP/LPPC, BSP 720, CH-1015, Lausanne, Switzerland*
[3] *On leave of absence from Bogolyubov Institute of Theoretical Physics, Kyiv, Ukraine*
[4] *INTEGRAL Science Data Center, Chemin d'Écogia 16, 1290 Versoix, Switzerland*
[5] *Geneva Observatory, 51 ch. des Maillettes, CH-1290 Sauverny, Switzerland*
[6] *Institut des Hautes Études Scientifiques, Bures-sur-Yvette, F-91440, France*

Received <date> ; in original form <date>

ABSTRACT
We find restrictions on the mass and mixing angle of the dark matter sterile neutrinos using X-ray observations of Coma and Virgo galaxy clusters.

1 INTRODUCTION

Recent experiments on neutrino oscillations (for a review see e.g. Strumia & Vissani (2005)) determine non-zero difference of masses of various species of neutrinos. The experiments on atmospheric neutrinos (Fukuda et al. 1998) are explained via $\nu_\mu \to \nu_\tau$ oscillations with mass difference $\Delta m^2_{\rm atm} = [2.2^{+0.6}_{-0.4}] \cdot 10^{-3}$ eV^2, while experiments (Ahmad et al. 2002; Eguchi et al. 2003) determine mass squared difference $\Delta m^2_{\rm sol} = [8.2^{+0.3}_{-0.3}] \cdot 10^{-5}$ eV^2 for $\nu_e \to \nu_{\mu,\tau}$ transitions. Probably, a simplest way to consistently explain these data is to add to the Standard Model several (at least two) gauge singlet fermions - right handed, or sterile neutrinos. However, the absolute values of masses of active and sterile neutrinos are not fixed by these experiments.

It was noticed long time ago (c.f. Dodelson & Widrow (1994)) that a sterile neutrino with the mass in the keV range appears to be a viable "warm" DM candidate. If such a neutrino is a main ingredient of the DM, it is potentially detectable in various X-ray observations. To wit, there exists a (sub-dominant) radiative decay channel of sterile neutrino N into active neutrinos ν_a and photon with energy $E = m_s/2$, with the width (Pal & Wolfenstein 1982; Barger et al. 1995)

$$\Gamma_{N\to\gamma\nu_a} = \frac{9\,\alpha\,G_F^2}{256\cdot 4\pi^4}\sin^2 2\theta\, m_s^5 = 5.5{\times}10^{-22}\theta^2\left[\frac{m_s}{1\,\text{keV}}\right]^5 \text{ s}^{-1}. \quad (1)$$

Here θ is the mixing angle defined as

$$\theta^2 = \frac{1}{m_s^2}\sum_{\alpha=\{e\mu\tau\}} |M_D|^2_{s\alpha} \quad (2)$$

with M_D being the Dirac mass and m_s is the sterile neutrino mass.

Although even for the main decay channel ($N \to 3\nu_a$) the lifetime of sterile neutrino must exceed the age of the universe, the decay $N \to \nu_a\gamma$ can result in a potentially detectable X-ray flux (Dolgov & Hansen 2002; Abazajian et al. 2001), since the density of DM in the universe is large. For example, the contribution to the diffuse X-ray background (XRB) can be comparable with measured XRB and is given by (see Boyarsky et al. (2005) and references therein)

$$F_{\rm XRB} \simeq \frac{\Gamma\rho^0_{\rm DM}}{2\pi H_0} \simeq 5\times 10^{-4}\,\theta^2\left[\frac{m_s}{1\,\text{keV}}\right]^5 \frac{\text{erg}}{\text{cm}^2\cdot\text{s}\cdot\text{sr}}\,, \quad (3)$$

where $\rho^0_{\rm DM}, H_0$ are the dark matter density in the universe and the Hubble constant. Neutrinos decaying at different red shifts produce a broad X-ray line with extended "red" tail. Such a feature in the XRB spectrum is, in principle, readily detectable (and distinguishable) from the broad-band continuum of observed XRB (Gruber et al. 1999). The non-detection of the DM decay feature in the XRB signal enables to put a bound on θ and m_s roughly at the level of (Boyarsky et al. 2005)

$$\Omega_s \sin^2(2\theta) \lesssim 3\times 10^{-5}\left[\frac{1\text{ keV}}{m_s}\right]^5\,, \quad (4)$$

where Ω_s is the present day density of sterile neutrino, understood as DM candidates.

Clustering of the DM at small red shifts results in the enhancement of the DM decay signal in the direction of large mass concentrations, such as galaxy clusters. Taking into account the typical overdensity $\mathcal{R} = \rho/\rho^0_{\rm DM}$ of a galaxy cluster is at the level of $\mathcal{R}\sim 10^3$, while typical cluster size is about $D \sim$ Mpc $\sim 10^{-3}H_0^{-1}$, one can find that the DM decay flux from a galaxy cluster,

$$F_{\rm cluster} = \frac{M^{\rm fov}_{\rm DM}\Gamma}{8\pi D_L^2} \quad (5)$$

($M^{\rm fov}_{\rm DM} \simeq \mathcal{R}\rho^0_{\rm DM} D D_\theta^2 \Omega^{\rm fov}$ is the mass of DM within telescope's field of view (FoV) and D_L, D_θ are the luminosity and angular diameter distances to the cluster) is comparable to the

background DM decay signal

$$\frac{F_{\rm cluster}}{F_{\rm XRB}} \sim \mathcal{R} D H_0 \sim 1 \, . \qquad (6)$$

Although the total DM decay flux from the XRB and from the cluster are of the same order, their spectra are different. The flux from the cluster would be detected as a narrow line whose width $\Delta E = \Delta E_{\rm det}$ is determined by the spectral resolution of an X-ray detector. At the same time, the DM decay contribution into XRB is produced by the decays at red shifts $z \sim 0 \div 1$ and, as a result the DM decay line is broadened to $\Delta E \sim m_s/2$. Thus, in spite of the fact that the compact DM sources at $z \simeq 0$ give just moderate enhancement of the DM decay flux, the enhancement of the signal in the narrow energy band centered on the line energy $E = m_s/2$ could be large. From the energy dependence of dF_{XRB}/dE (see e.g. Boyarsky et al. (2005)) one can estimate that the enhancement can be by a factor of $m_s/\Delta E_{\rm det} \sim 10 - 100$ for instruments of spectral resolution of Chandra or XMM (in this paper we will use XMM observations of Virgo and Coma clusters).

However, the detection of the DM decay line in the galaxy clusters is complicated by the fact that most of the galaxy clusters show strong continuum and line emission from the hot intracluster gas. The typical temperatures of the intraculser gas,

$$T_{\rm gas} \sim G \, \mathcal{R} \rho^0_{\rm DM} D^2 m_p \sim 10 \left[\frac{\mathcal{R}}{10^3}\right] \left[\frac{D}{1 \text{ Mpc}}\right]^2 \text{ keV} \, , \qquad (7)$$

lie exactly the range of *Chandra* or XMM-Newton satellites – 1-10 keV. In fact, for a typical nearby X-ray bright cluster, the diffuse continuum emission from the cluster core is by a factor $\sim 10^2 - 10^3$ stronger than the XRB emission from behind the core. Thus, the factor $10-100$ increase of the flux in the DM decay line from the cluster direction is "washed out" by the strong increase of the X-ray continuum emission from the direction of a cluster. We will see however than in spite of such a strong background, the bound on $\sin^2 2\theta$ can be improved by a factor of about 2–4 in comparison with XRB (4).

Previously this question was addressed in the paper by Abazajian et al. (2001); Abazajian (2005). There the authors claimed the following limit on the neutrino mass and mixing angle, derived from the non-observation of the DM decay line from the center of the Virgo galaxy cluster: $\sin^2(2\theta) \lesssim 1.0 \times 10^{-5} (\text{keV}/m_s)^4$ for $1 < m_s < 10$ keV. This limit is several times better than Eq. (4).

In this paper we re-analyze the bounds on the sterile neutrino mass and mixing angle imposed by the observations of Coma and Virgo galaxy clusters. As we will discuss in Section 4, our constraints are weaker than those claimed by Abazajian et al. (2001); Abazajian (2005). We will compare in details these two results in Section 5 and explain the origin of the difference.

In this work we show that the problem of the large continuum X-ray emission from the cluster core can be partially relaxed, if one searches for the DM decay signal from a region outside the bright X-ray core of the cluster. The reason for that is the following: outside the core of the cluster, the surface brightness profile of intracluster medium (ICM) behaves as $\mathcal{S}(r) \sim r^{-\alpha}$ (where, e.g. for Virgo cluster $\alpha \sim 1.6$ (Fabricant & Gorenstein 1983; Schindler et al. 1999; Young et al. 2002)), while the surface brightness profile of the DM is more shallow $\mathcal{S}_{\rm DM}(r) \sim r^{-1}$ (see e.g. Cavaliere & Fusco-Femiano (1976), for mass density of Virgo cluster). Therefore, by moving away from the center, one can put much tighter constraints on the DM parameters. For the case of Coma cluster observations with XMM one needs to use periphery observations ("coma mosaic" observations, performed in May-June 2000, (Briel et al. 2001; Neumann et al. 2003)). For the case of Virgo this goal can be achieved already for the XMM observation of M87 (observation ID 0114120101) Indeed, as the core radius of Virgo cluster is very small ($r_0 \lesssim 1.6'$), the existing observations with XMM EPN camera (field-of-view $\sim 15'$) allows one to study properties of Virgo cluster till about $10 r_0$. We also show that the bound can be further improved if the X-ray spectra of galaxy clusters are analyzed by the method proposed by Boyarsky et al. (2005) for the search of the DM decay line in the XRB spectrum. We describe the analysis of the data from Coma and Virgo observations in Section 3 and present results in Section 4.

2 DM DECAY LINE VS. THERMAL BREMSSTRAHLUNG EMISSION.

The main obstacle for improving the bound on the neutrino parameters from the X-ray background by using galaxy clusters observations is strong X-ray continuum and line emission from the cluster core. In this Section we show that this obstacle could be partially avoided if one extracts the X-ray spectrum from the regions beyond the core of the continuum X-ray emission. The idea is that the radial surface brightness profile of the continuum emission is normally steeper than the radial surface brightness profile expected from the DM decay line.

Indeed, the surface brightness profile of a relaxed cluster of galaxies is usually well-fitted by the so-called isothermal β-model (Cavaliere & Fusco-Femiano 1976; Sarazin & Bahcall 1977):

$$\mathcal{S}(r) = \frac{\mathcal{S}_0}{(1 + (r/r_0)^2)^{3\beta - 0.5}} \, , \qquad (8)$$

where r is the *projected* distance from the center of the cluster, $\mathcal{S}_0$ is the overall normalization factor and r_0 is the "core radius" of the region of X-ray emission. Parameters $\mathcal{S}_0$, r_0 and β are different for different clusters (see Section 3 below).

The volume emissivity of the intracluster gas which results in the surface brightness profile (8) is

$$\mathcal{V}(\boldsymbol{r}) = \frac{\mathcal{V}_0}{(1 + (\boldsymbol{r}/r_0)^2)^{3\beta}} \, , \qquad (9)$$

where $\boldsymbol{r}$ is the (3d) distance to the center of the cluster. The continuum X-ray emission from the intracluster gas is the thermal bremsstrahlung for which the volume emissivity is proportional to the square of the gas density. The radial density profile of the hot intracluster gas is therefore

$$n_{\rm gas}(\boldsymbol{r}) = \frac{n_0}{(1 + (\boldsymbol{r}/r_0)^2)^{3\beta/2}} \sim \sqrt{\mathcal{V}(\boldsymbol{r})} \, . \qquad (10)$$

To calculate the radial mass profile $M(r)$ (gas plus galaxies plus the DM) of the cluster one has to make an assumption that the intracluster gas is in hydrostatic equilibrium (Cavaliere & Fusco-Femiano 1976; Sarazin & Bahcall

1977). One can really expect this assumption to hold only for relaxed galaxy clusters, but as it turns out even for e.g. Virgo this model gives good predictions (c.f. Nulsen & Bohringer (1995)). Under this assumption the overall mass profile can be calculated from the Newton's law

$$\frac{dp}{d\boldsymbol{r}} = n_{\rm gas}(\boldsymbol{r})\frac{dT(\boldsymbol{r})}{d\boldsymbol{r}} + T(\boldsymbol{r})\frac{dn_{\rm gas}(\boldsymbol{r})}{d\boldsymbol{r}} = -\frac{GM(\boldsymbol{r})n_{\rm gas}(\boldsymbol{r})}{\boldsymbol{r}^2}\ , \tag{11}$$

where $T(\boldsymbol{r})$ is the radial temperature profile of the hot intracluster gas. In the region where the temperature does not change significantly, one can calculate the overall mass profile analytically by substituting (10) into (11). The assumption of hydrostatic equilibrium them immediately leads to the following total mass dependence on the distance $\boldsymbol{r}$ from the center of the cluster (Cavaliere & Fusco-Femiano 1976; Sarazin & Bahcall 1977)

$$M(\boldsymbol{r}) = 1.13\times10^{14}M_\odot\,\beta\frac{T}{1\ \text{keV}}\frac{\boldsymbol{r}}{\text{Mpc}}\frac{(\boldsymbol{r}/r_0)^2}{1+(\boldsymbol{r}/r_0)^2}\ . \tag{12}$$

The overall density profile is given by

$$\rho_{\rm total}(\boldsymbol{r}) = \rho_{0,\rm total}\frac{3+(\boldsymbol{r}/r_0)^2}{\left(1+(\boldsymbol{r}/r_0)^2\right)^2}\ . \tag{13}$$

In the first approximation one can estimate the DM density as $\rho_{\rm DM} = \kappa\rho_{\rm total}$ with $\kappa \lesssim 1$.

The surface brightness profile (8) should be compared with the surface brightness of the DM. Integrating the volume emissivity of the DM decay line over the line of sight one can find the brightness profile of the DM decay line

$$\mathcal{S}_{\rm DM}(r) = \frac{\Gamma m_s \mathcal{N}_{\rm DM}(r)}{8\pi D_L^2}\ , \tag{14}$$

where $\mathcal{N}_{\rm DM}(r) = 2\int_0^\infty dz\, n_{\rm DM}(\sqrt{r^2+z^2})$ is the column density of the DM as a function of the distance from the cluster center. Substituting $\rho_{\rm total}$ from (13) one obtains

$$\mathcal{S}_{\rm DM}(r) = \frac{\Gamma\rho_{0,\rm DM}r_0}{D_L^2}\left[\frac{2+(r/r_0)^2}{8(1+(r/r_0)^2)^{3/2}}\right]\ . \tag{15}$$

Integrating $2\pi r\mathcal{S}_{\rm DM}(r)$ (15) from $r=0$ to some r one finds the flux of DM from a FoV circle with the projected radius r:

$$F_{\rm DM}(r) = \frac{\pi}{4}\frac{\rho_{0,\rm DM}r_0^3\Gamma}{D_L^2}\,g(r/r_0)\ , \tag{16}$$

where we have defined a *geometry factor* $g(r)$, describing that part of the cluster, which we are using for the measurement. In case of the circular region with the projected radius r one gets from (15):

$$g(r/r_0) = \frac{(r/r_0)^2}{\sqrt{1+(r/r_0)^2}}\ . \tag{17}$$

One can see that $\mathcal{S}_{\rm DM}(r)\sim r^{-1}$ for $r\gg r_0$. Thus, the radial profile of DM decay line is significantly more shallow than the profile of the continuum X-ray emission from the hot intracluster gas:

$$\frac{\mathcal{S}_{\rm DM}}{\mathcal{S}_{\rm gas}} = \frac{\mathcal{S}_{\rm DM}(0)}{\mathcal{S}_{\rm gas}(0)}\left[2+\frac{r^2}{r_0^2}\right]\left[1+\frac{r^2}{r_0^2}\right]^{3\beta-2} \sim \left(\frac{r}{r_0}\right)^{6\beta-2},\ r\gg r_0\ . \tag{18}$$

As it is clear from Eq. (8), $\beta<\frac{1}{6}$, therefore, the share of DM contribution to the total brightness (at energy $E=m_s/2$) increases as one moves away from the center of a cluster.

3 DATA ANALYSIS

In this work we have chosen to analyze data of XMM-Newton observations of Virgo galaxy cluster (observation ID 0114120101, June 2000) and Coma cluster. For the latter we have taken two observations which constituted the part of the so called *Coma mosaic* (Briel et al. 2001; Neumann et al. 2003): that of the center of Coma cluster (observation ID 0124711401, May 2000) and one of the peripheral observations ("Coma 3", ID 0124710301, June 2000).

3.1 "Total flux" restrictions.

First, we find the restrictions on the parameters of sterile neutrino, based on the total emission from the ICM. Namely, using the XMM observation data and estimating a mass of DM in the center of a cluster as in Section 2, we restrict parameters m_s and $\sin^2(2\theta)$ by demanding that the flux of DM decay line (16) did not exceed the total flux in the energy bin, equal to the 3σ where with of the Gaussian line σ is equal to the spectral resolution of XMM. We will often dub this method simply *total flux restrictions*. This method provides the most robust exclusion.

3.1.1 Analysis for Coma cluster

To find the typical numerical values of the DM decay flux as compared to the thermal bremsstrahlung flux, let us use the parameter values for the Coma galaxy cluster. Its surface brightness profile is well defined by the β-model (8) with $\beta=0.75$ and $r_0 = 10.5' = 0.3$ Mpc[1] (see e.g. Briel et al. (1992); Neumann et al. (2003)). The virial mass of Coma cluster, contained in the virial radius $r^{\rm vir}_{Coma} = 3.5$ Mpc is $M^{\rm vir}_{Coma} = 1.3\times10^{15}$ M$_\odot$ (Briel et al. 1992). Substituting these numbers into Eqs. (12)–(13) and taking fraction of gas in the Coma cluster 18% (Briel et al. 1992) one finds that

$$\rho_{0,\rm DM} \simeq 3\times10^{14}\ \frac{\text{M}_\odot}{\text{Mpc}^3}\ . \tag{19}$$

Substituting these values in Eq. (16) one finds that the flux of DM from a FoV circular region with projected radius r is given by

$$F_{\rm DM,Coma} \simeq 6.7\times10^{-8}\,\theta^2\left[\frac{m_s}{1\ \text{keV}}\right]^5 g(r)\frac{\text{erg}}{\text{cm}^2\cdot\text{s}}\ , \tag{20}$$

where $g(r)$ is given by Eq.(17). Flux (20) should be compared with the emission of the ICM in the Coma center region. We use observation of Coma center with EPN camera of XMM-Newton satellite (observational ID 0124711401) to extract flux per energy bin, equal to the spectral resolution of XMM ($\Delta E_{\rm det}\sim200$ eV) in the interval 0.5-10 keV. The geometry factor for the circle of $700''$ is equal to 0.82. The resulting restriction on m_s and $\sin^2(2\theta)$ is shown on Fig. 1 in the red solid line. Qualitatively this result can be described as follows. The flux (per energy bin) from Coma center[2] at 1 keV $F_{1\ \rm keV} = 1.62\times10^{-11}$ erg/cm$^2\cdot$s

[1] We take $h=0.71$ and the distance to the Coma cluster $D_L=98$ Mpc (red-shift $z=0.023$).

[2] Compare Briel et al. (1992): $F_{1\ \rm keV}\simeq1.1\times10^{-11}erg/cm^2\cdot$s in 200 eV energy bin.

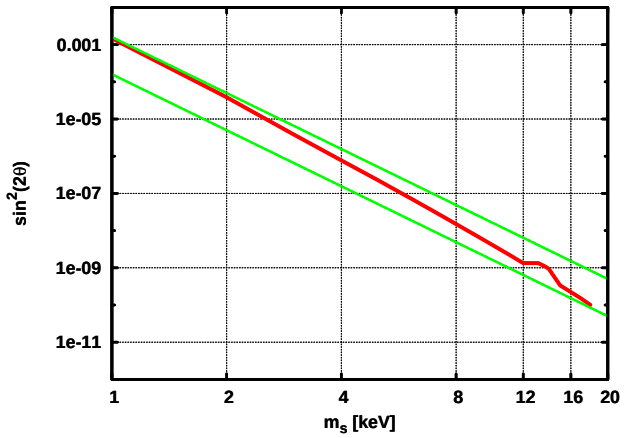

Figure 1. Exclusion plot from the total flux restriction from the circular region with radius 700′′ in the center of Coma cluster. The straight green lines represent $\sin^2(2\theta) m_s^5 = \text{const}$ lines, corresponding to the total flux at energies 1 keV and 10 keV (in the 200 eV energy bin).

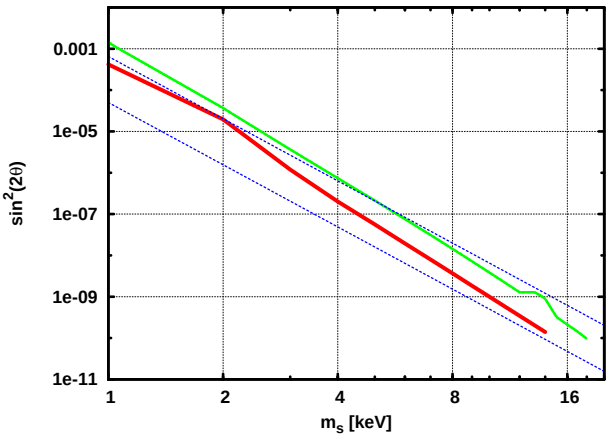

Figure 2. Exclusion plot based on the restrictions derived from a total flux from Coma 3 peripheral observation (red solid line) as compared with Coma center (green line, identical to the red curve on Fig. 1). Thinner blue lines represent $m_s^5 \sin^2(2\theta) = \text{const}$ with normalization corresponding to fluxes at 1 keV and 7 keV.

is about an order of magnitude bigger, than that at 10 keV $F_{10\,\text{keV}} = 2.5 \times 10^{-12}$ erg/cm$^2 \cdot$ s. The flux of DM Eq. (20) is bounded by these two fluxes and exclusion curve in the space (m_s, $\sin^2 2\theta$) is bounded by the two straight lines $m_s^5 \sin^2(2\theta) = \text{const}$ (dashed lines on Fig. 1), where *const* is defined (via Eq.(20)) by the fluxes $F_{1\,\text{keV}}$ and $F_{10\,\text{keV}}$ correspondingly.

3.1.2 Coma periphery

As discussed in Section 2, to improve the bound on total flux, we move away from a center of the cluster. Unfortunately, modern X-ray telescopes are normally "narrow FoV" instruments and, e.g. the XMM pointing toward the center of Coma cluster covers only the region of the size $r \sim r_0$. Therefore we use one of the observations from Coma mosaic (May-June 2000) (Briel et al. 2001; Neumann et al. 2003). Although the flux from Coma 3 periphery falls by a factor 20, as compared to the Coma center[3], we see that relative change between 1 keV and 10 keV is again an order of magnitude (c.f. Fig. 3). For Coma 3 observation (distance between the centers of two observations is 39′ and FoV radius is $\sim 12'$), the geometry factor in Eq. (20) is equal to $g_{\text{Coma3}} = 0.18$ which improve an exclusion plot Fig. 2 by about factor of 5.

3.1.3 Analysis for Virgo cluster

We repeat the analysis of the previous Section for the case of center of Virgo cluster (M87). For this cluster again the surface brightness is well-fitted by the β-model with $\beta \simeq 0.4$ and core radius[4] $r_0 \simeq 1.6' = 8$ kpc and $S_0 = 5 \times 10^{-12} \frac{\text{erg}}{\text{cm}^2 \cdot \text{s} \cdot \text{arcmin}^2}$ (Fabricant & Gorenstein 1983; Young et al. 2002). The mass in the center of the Virgo cluster can be described by the isothermal β-model

[3] For Coma 3 observation $F_{1\,\text{keV}} = 2 \times 10^{-12}$ erg/cm$^2 \cdot$ s, $F_{10\,\text{keV}} \sim 10^{-13}$ erg/cm$^2 \cdot$ s.

[4] We adopt the distance to M87 $D_L = 18$ Mpc ($z = 0.0044$)

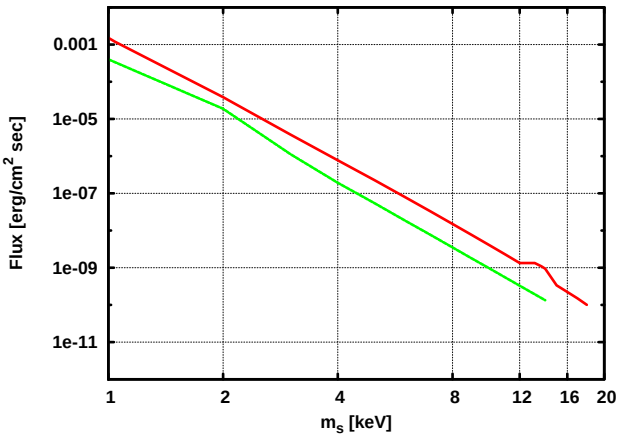

Figure 3. Comparison between Coma center (red curve) and Coma 3 (green curve) fluxes (per 200 eV energy bin).

(see e.g. Nulsen & Bohringer (1995)). Using various measurements of the mass distribution in the center of the Virgo cluster (Nulsen & Bohringer 1995; Evrard et al. 1996; McLaughlin 1999), we obtain

$$\rho_{0,\text{DM}} \simeq 6 \times 10^{16} \frac{\text{M}_\odot}{\text{Mpc}^3} \tag{21}$$

and correspondingly flux from the FoV circle with (projected) radius r is given by

$$F_{\text{DM,M87}} \simeq 7.7 \times 10^{-9}\, \theta^2 \left[\frac{m_s}{1\,\text{keV}}\right]^5 g\left(\frac{r}{r_0}\right) \frac{\text{erg}}{\text{cm}^2 \cdot \text{s}}\,. \tag{22}$$

The geometry factor $g(r)$ is defined in (17).

Using the M87 observation by XMM-Newton (ID 0114120101), we extract the total flux from the central 11′ of the EPN FoV (centered at M87 galaxy).[5] The geometry factor for this case is $g_{M87}(11') = 6.8$.

Using expression (22) for the flux of DM we get a

[5] The actual experimental data is shown on Fig. 9 in red line

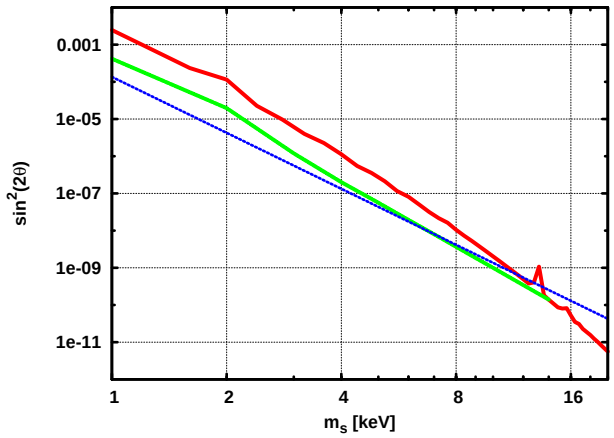

Figure 4. Restrictions based on the total flux from the circle with the radius 11′ with the center at M87 (red line). Green line represents the data for Coma periphery – same as on Fig. 2. Blue line – restriction (4) from Boyarsky et al. (2005).

restriction on parameters of sterile neutrino. The thermal bremsstrahlung of ICM around M87 has temperature about $T = 2.54$ keV, which is about 4 times smaller than that for the Coma cluster. Therefore, the flux drops by about two orders of magnitude between 1 keV and 10 keV.[6] This leads to an exclusion plot, which is weaker than that from a Coma periphery at small energies, but gets stronger, than the former restriction at masses $m_s \gtrsim 12$ keV, as shown on Fig. 4.[7]

3.1.4 Virgo periphery

As we said above, in general periphery of the cluster does not fit into one XMM FoV. However, Virgo cluster is a special case in this respect. Indeed, in spite of the fact that Virgo cluster is the closest to us galaxy cluster, the angular size of its core is rather small by the cluster scales. The surface brightness of the core of the Virgo cluster radius $r_0 = 1.6'$ Fabricant & Gorenstein (1983); Young et al. (2002) and thus the FoV of the XMM EPN camera covers about $10r_0$. Nevertheless, the ratio of $\mathcal{S}_{\rm gas}/\mathcal{S}_{\rm DM}$ is changing rather slowly – as $(r/r_0)^{-0.58}$

On the other hand, taking ring (with the radii 9′ and 11′), rather than the full circle with the radius $\sim 11'$ leads to the decrease of the geometric factor in Eq. (22) by a factor of about 5, which compensates the gain almost entirely and therefore, moving away from the center does not improve the restriction, based on the total flux from the vicinity of M87.

[6] The measured flux at 1 keV is $F_{1\ \rm keV} \simeq 4.8\times10^{-11}$ erg/cm$^2\cdot$ s. This number should be compared with the one, obtained from the surface brightness profile of Fabricant & Gorenstein (1983), $F \simeq 4.3\times10^{-11}$ erg/cm$^2\cdot$ s.

[7] One should take all total flux restrictions at the energies above bremsstrahlung cut-off with the grain of salt. Indeed, as will be discussed in more details in Section 3.2.1–3.2.2, the uncertainties of measurement of this flux is comparable with the flux itself.

3.2 Statistical analysis of the XMM data

In order to further improve the bounds on the sterile neutrino parameters (as compared to Sections 3.1), we apply the method suggested in Boyarsky et al. (2005). Namely, we use the fact that the spectral shape of the DM decay line may differ significantly from that of the ICM continuum and therefore adding a line which is "too strong" (e.g. with the flux equal to that of the continuum) will simply contradict observations.

In general, typical X-ray spectrum of a galaxy cluster is dominated by the bremsstrahlung continuum and line emission from the hot intracluster gas. To obtain a good fit of observed data to physical model (such as e.g. MEKAL (Mewe et al. 1986; Liedahl et al. 1995) or Raymond-Smith (Raymond & Smith 1977)), one needs to take into account that their parameters (e.g. temperature and abundances) vary with radius and even with azimuthal angle; that the ICM plasma is often described by multi-component models; etc. Therefore, often the sophisticated data analysis is required to extract the "best-fitting" parameters for these models and one can only fit these models to the data, coming from small annular sectors of the FoV.

However, for our purposes one needs *any* "best-fit" model to the data, gathered from previously described annular or circular regions of FoV. We are not interested in values or distributions of temperatures, abundances, etc. of the ICM plasma. Rather, we want to put restrictions on parameters of the sterile neutrino, based on *non-detection* of the presence of the decay line against an emission background. Both from experimental data and from theoretical models, one can see that X-ray spectrum of galaxies has a form of continuum plus separate lines. Knowledge of physics (the correct choice of model) allows to relate various parameters of the model (such as positions and intensities of the lines, abundances, etc.) to each other, however, the structure of the model remains the same: continuum emission plus lines.

Therefore, we introduce a phenomenological model for the cluster spectrum which provides a good fit to the X-ray data, but at the same time has a limited number of parameters so that one can easily constrain the maximal possible contribution of the DM decay line into the X-ray emission from the cluster. The restriction is much stronger in those regions of the spectrum, where one has no lines – the non-detection of the decay line against monotonic continuum, essentially puts the restriction on the flux of the line comparable to the error of the continuum flux. At the regions, where emissions lines are present, the restriction of statistical analysis is much weaker and the flux of DM decay is essentially equal to the excess flux above the continuum.

The models and method of their construction are described in Appendices A–C. These models provide a satisfactory fit to the observed X-ray spectra of Coma and Virgo clusters. Obviously, addition of a strong line feature with the integrated line flux equal to the model flux within a given energy bin would destroy the fit to the data. Moreover, it would provide a non-satisfactory fit already at much smaller DM line flux, of the order of the statistical error of the data in the narrow energy bin.

In order to quantify the above qualitative observation we use the following algorithm to find the maximal possible contribution of the DM decay line at a given energy:

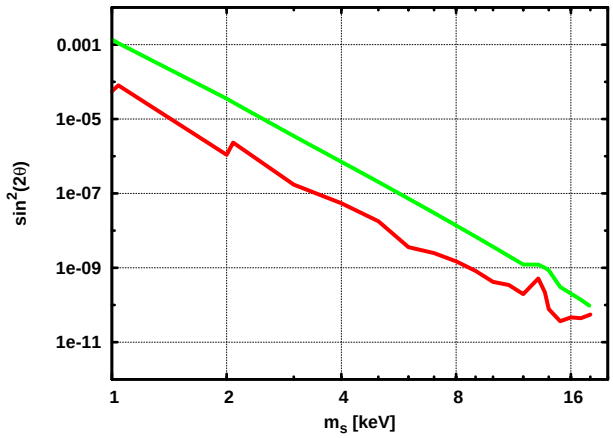

Figure 5. Red line: exclusion plot based on statistical analysis from Coma center observation (circular region of the radius 700′′ around the center of the cluster). Green line – restriction based on the total flux from the same region (curve from Fig. 1).

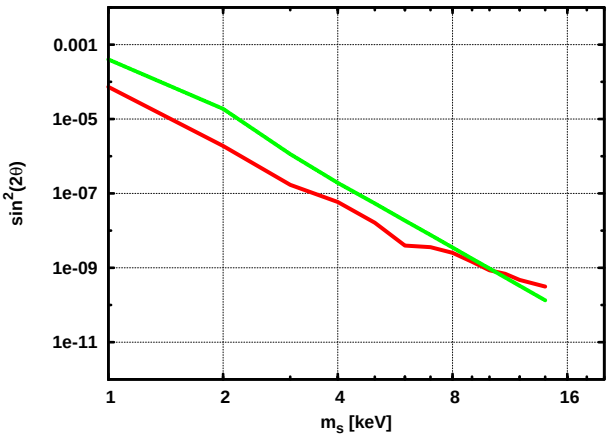

Figure 6. Red line: exclusion plot based on statistical analysis from Coma 3 peripheral observation of Section 3.1.2. Green line – restriction based on the total flux from the same region (curve from Fig. 2).

(i) We fix the parameters of a phenomenological model to their best fit values.

(ii) We introduce an additional model component which is a Gaussian line at the energy E_0 with the width ΔE equal to the energy resolution of the instrument ($70-150$ eV for XMM EPN camera and $15\%(E/60\text{ keV})^{-0.5}$ for Beppo-Sax PDS).

(iii) Then we increase the normalization of the additional Gaussian until it starts to distort the overall fit to the data. As a simple criterium for this we use the increase of reduced χ^2, which leads to the vanishingly small *null hypothesis probability*. The actual value of $\Delta\chi^2$ depends of course on the number of degrees of freedom and has to be chosen individually for every data set. We confirm by the visual inspection that for such a distortion, fitted model does not follows the data anymore in the region of $E\sim E_0$.

(iv) We make a "scan" over the line energy 0.5 keV $\leqslant E_0 \leqslant$ 10 keV (and 15 keV $\leqslant E_0 \leqslant$ 40 keV for Beppo-Sax data) to find the maximal possible normalization of the Gaussian as a function of energy.

As discussed above and in Boyarsky et al. (2005), the only assumption about the empirical model, which we make, is that the power-law regions of the spectrum are actual monotonic bremsstrahlung and do not contain "dips" see Fig. A1b.

In the Sections 3.2.1– 3.2.2 below we compare this method with that of the Section 3.1 for the case of Coma and Virgo cluster.

3.2.1 Bounds from statistical analysis of the Coma cluster observations.

The simple model for Coma center X-ray emission is provided in Appendix A. The results of statistical analysis (and demonstration of its improvement over the total flux restrictions) are shown on the Fig. 5. One can see that overall one gets about an order of magnitude improvement over the results of Section 3.1.1. One can also see "spikes" at $E\simeq 1$ keV, $E\simeq 6.5$ keV, etc. ($m_s\simeq 2$ keV,13 keV,etc.) – positions of the strong emission lines in the Coma spectrum (see Appendix A for their identification). This is expected. Adding a line in the energy region where data is monotonic and well described by the smooth power-law bremsstrahlung emission distorts the fit much more than adding the line with the same strength to the region of multiple element emission lines.

Similarly, the results of statistical analysis of the data from Coma 3 region are shown on Fig. 6. Here, the improvement is not so drastic as in case of Fig. 5. The reason for that is obvious – the statistics for Coma 3 is lower and therefore the fitted curve can be distorted stronger, without spoiling reduced χ^2 too much. From looking at the Fig. 6 one can see that the proposed statistical analysis is in some sense complimentary to that of the total flux analysis: namely, while it is stronger at small masses ($m_s\lesssim 10$ keV, it gets more and more weak as m_s increases – tendency which is quite opposite to that of the total flux restriction. The reason for that is clear – at large energies there is almost no X-ray emission from cluster, and the difference between a very weak signal from X-ray emission and background has very large uncertainty. Therefore, total flux restriction for $m_s\gtrsim 10$ keV is provided only for illustrative purposes and the results of the statistical analysis should be considered as a correct limit.[8]

3.2.2 Bounds from statistical analysis of the of Virgo cluster.

Let us apply the same strategy to the XMM pointing toward M87/Virgo cluster. For this we consider the spectrum collected from a thin ring $9'<r<11'$ around the M87. We attempt to add a DM decay line to the resulting spectrum, described in Appendix C and find the maximal strength of the line that does not deform the spectral fit (in the sense described in the previous sections). The resulting exclusion plot is shown by the dashed lines in Fig. 7. We see that the

[8] We have used the Beppo-Sax observation of Coma cluster, to obtain constraints in the range 15 keV $\leqslant E\leqslant$ 40 keV. The obtained restrictions (both statistical and "total flux") are about an order of magnitude weaker than restrictions from XRB.

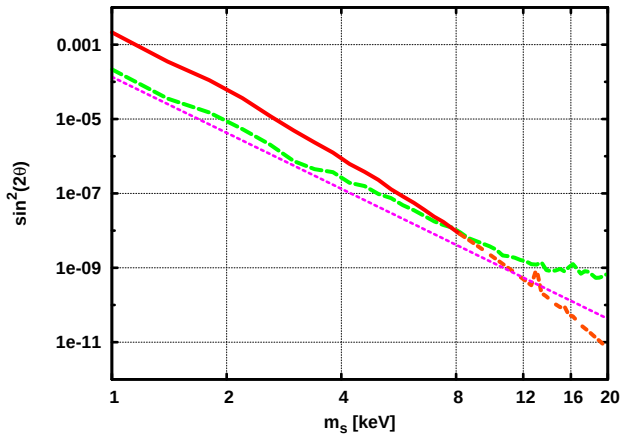

Figure 7. Restrictions from the statistical analysis of the periphery (ring $9'$–$11'$) around the M87 (green dashed line). This restriction is about an order of magnitude better that the one, coming from the total flux, measured from the same region (red solid line) at small energies ($m_s \lesssim 8$ keV and then become worse (red dashed line), as statistical error of the data grows. This is due to the fact that for $E \gtrsim 4$ keV total flux is measured with uncertainty comparable or exceeding the flux itself. The straight line represent the XRB restrictions (4).

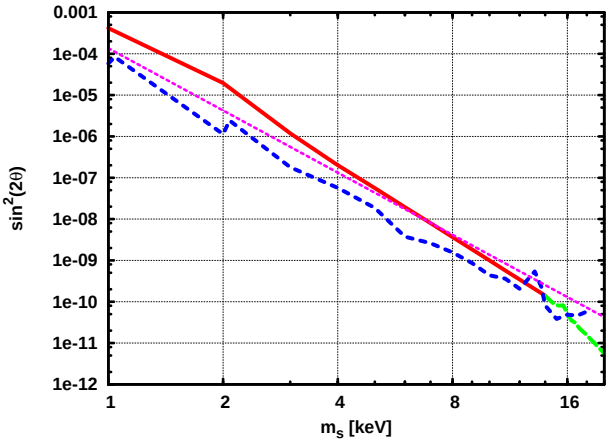

Figure 8. Exclusion plot for parameters of sterile neutrino, based on analysis of the cluster of the Coma and Virgo clusters of galaxies. The red solid line represents the restriction, coming from the Coma periphery ("Coma 3") observation, while the green dashed line, coming from observation of Virgo cluster, provides stronger restriction for $m_s \gtrsim 14$ keV. The blue dashed curve represents the result of statistical analysis of the Coma center. The straight magenta line represents the XRB restrictions from Boyarsky et al. (2005).

statistical analysis improves the restrictions over that of the total flux for small masses (i.e. for which $E = m_s/2 \lesssim T$, where $T \sim 2.5$ keV is the temperature of the ICM for the center of the Virgo cluster, while gets significantly worse for higher energies. As discussed in Section 3.2.1, this is due to the fact that the errors in flux are comparable (or even exceed) the flux itself and therefore the results of the statistical analysis should be considered as the correct limit.

One can also see that the restriction from the Virgo is not as strong as the one, which we obtained from the Coma center (shown on Fig. 5). This is due to the same reason as above: Coma cluster has higher temperature and the data, collected from a large field, has bigger statistical significance, hence smaller errors.

4 RESULTS

In this Section we summarize the restrictions on parameters of sterile neutrino, obtained from analysis of the Virgo and Coma cluster of galaxies. Based on analysis of the core and peripheral regions of these clusters we obtain the following results:

(i) The most robust restriction is based on the requirement that the flux of DM did not exceed the total X-ray flux in the given energy bin (chosen to be $\Delta E = 200$ eV in our case). The best restriction comes from the observation of the Coma periphery (XMM-Newton observation "Coma 3" (ID 0124710301) with EPIC EPN camera). It provides an exclusion plot, shown in the solid red line on the Fig. 8.

(ii) For $m_s \gtrsim 14$ keV, the restriction from the Virgo cluster becomes stronger (due to the fact, that the temperature of the intracluster gas in the Virgo cluster is several times lower, than that of the Coma. This results in an improvement, shown in the green dashed line, continuing previous bound above $m_s \simeq 14$ keV on Fig. 8.

(iii) By analyzing the form of the spectrum, one can refine the restrictions on parameters of sterile neutrino (as discussed in details in Section 3.2). From all the data used in this work, the best result was obtained in analysis of the Coma center region (see Section 3.2.1 and Appendix A). The resulting exclusion region is shown as dashed blue line on the Fig. 8. It provides an improvement by a factor 2–4 over the XRB result of Boyarsky et al. (2005) in the region 2 keV $\lesssim m_s \lesssim$ 10 keV. One can qualitatively understand why Coma center observations gives the best result for statistical analysis. As discussed in the Section 3.2.1, the more monotonic is the data, the better the method of statistical analysis works. The result significantly improves over the total flux restriction only in the regions where "there are no lines". Due to the fact that Coma temperature is 4 times bigger than that of Virgo, the phenomenological model for the Coma cluster requires only three additional lines (as discussed in details in Appendix A).

5 DISCUSSION.

In this work we analyzed the restrictions on the parameters of the sterile neutrino, as a dark matter candidate, coming from the observations of several clusters of galaxies. Below we compare our results with those of other authors and discuss what improvements on restriction plots one expects to obtain from galaxy clusters data.

(i) We see that this work brings improvement by a factor 2–4 (in the region 2 keV $\lesssim m_s \lesssim$ 10 keV) over the previous analysis of Boyarsky et al. (2005) (see Fig. 8). This should be compared with the results of Abazajian et al. (2001); Abazajian (2005), where stronger constraints, derived from the restriction of the total flux of the Virgo cluster, were claimed. Below, we explain the reason for this difference.

Assuming $\theta \simeq 6 \times 10^{-5}$, Abazajian et al. (2001) argued that if the sterile neutrino mass would be $\gtrsim 5$ keV, the "enormous" DM decay line observed in the core of Virgo galaxy cluster (or, more precisely from its cD galaxy M87) would dominate over the continuum flux. To illustrate this, Abazajian et al. (2001) modeled (via WEBSPEC interface) the emission of the M87 by MEKAL model with the temperature $T = 2.5$ keV and overall normalization of the flux in the 2-10 keV interval equal to 1.5×10^{-12}erg/(cm$^2\cdot$s), the number taken from Boehringer et al. (2001). This value for the emission flux from the center of Virgo is, however, two orders of magnitude *below* the actual flux, as one can see from the literature (Fabricant & Gorenstein 1983; Arnaud & Evrard 1999) or by comparing these numbers with the actual experimental data (e.g. observation of M87 with XMM in 2001 (obs. ID 0114120101). From the latter one can measure that the flux in the range 2-10 keV is some two orders of magnitude higher ($\sim 10^{-10}$ erg/cm$^2\cdot$s). While the discussed in the paper of Abazajian et al. (2001) flux of DM is taken from the whole FoV of Chandra (which has an area ~ 300 arcmin^2), the number 1.5×10^{-12} erg/cm$^2 \cdot$ s in the Boehringer et al. (2001) refers to the emission from the active nucleus of the central galaxy of Virgo cluster, M87, collected from the central 10 arcsec of the XMM (not Chandra) field of view. For the mixing $\theta \simeq 6 \times 10^{-5}$, used in Abazajian et al. (2001), the flux of DM is about two orders of magnitude below the MEKAL flux in the energy bin around $E = m_s/2 = 2.5$ keV (see Fig. 9). In the later work Abazajian (2005), the same data was used to provide an exclusion plot in the (m_s, $\sin^2 2\theta$) parameter space of the form $\sin^2(2\theta) \lesssim 1.0 \times 10^{-5} (\text{ keV}/m_s)^2$.

(ii) Statistical analysis of the Coma center and Coma 3 data, gave very close restrictions. However, Coma 3 represents only one of the observations of Coma mosaic, which cover the annular region between $\sim 10'$ and $40'$ around the center of the Coma cluster. By combining these results, one effectively increases observation time by about a factor of 10. This should lead to the modest improvement of the statistical restriction by about $\sqrt{10}$. We leave this for the future work.

(iii) The restrictions, based on the total flux, can be improved if one moves to the periphery of the cluster. The farther away from the center one moves, the stronger becomes "signal-to-background" ratio (especially in the case of the Coma cluster, c.f. Eq. (18)). Therefore, one should try to move away from the center of the cluster. The maximal distance where one can move i restricted by the requirement that the DM decay line is still stronger, than the XRB background (otherwise one does not gain anything, compared to the restriction (4) from XRB).

(iv) At the energies above 15 keV, other missions (such as INTEGRAL) should be used to obtain the restrictions on parameters of sterile neutrino.

Acknowledgements

We would like to thank K. Abazajian and I. Tkachev for useful comments. The work of M.S. was supported in part by the Swiss Science Foundation. The work of O.R. was supported in part by European Research Training Network contract 005104 "ForcesUniverse" and by a *Marie Curie International Fellowship* within the 6$^{\text{th}}$ European Community Framework Programme.

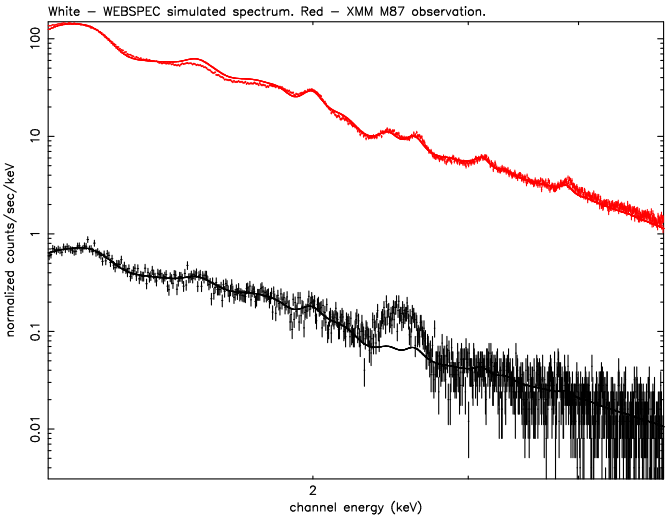

Figure 9. Comparison of WEBSPEC simulations of Abazajian et al. (2001) (lower black line) with actual XMM observation of M87 – red line.

APPENDIX A: SIMPLE MODEL FOR THE X-RAY SPECTRUM OF THE CORE OF COMA CLUSTER.

The simple phenomenological fit to the XMM-Newton PN and Beppo-SAX PDS data is shown in Fig. A1. The model consists of a powerlaw with a photon index $\Gamma = 1.36 \pm 0.04$ modified at high energies by an exponential cutoff with the cut-off energy $E_{cut} = 8.3 \pm 0.7$ keV and by the absorption with column density $N_H = (1.5 \pm 0.3) \times 10^{20}$ cm^{-2} (which is roughly the galactic absorption in the direction of Coma cluster). Several bright X-ray lines are visible in addition to the cut-off powerlaw component. They are the red-shifted 6.7 keV and 7.0 keV Fe Kα and Kβ lines as well as 0.5 keV and 1.0 keV O and Ne lines. All the components of the model are shown together with the unfolded 0.3-50 keV spectrum of the central part of the Coma cluster in the right panel of Fig. A1. The reduced χ^2 of the fit is $\chi^2 = 1.04$.

APPENDIX B: SIMPLE MODEL FOR THE X-RAY SPECTRUM OF THE CORE OF VIRGO CLUSTER.

Modeling the spectrum of the central part of Virgo cluster turns out to be more complicated because more lines are evident in the 1-5 keV part of the spectrum. This can be explained by lower, compared to Coma, temeperature of Virgo cluster, $T \simeq 2 - 3$ keV. Besides, Virgo cluster is a "cD galaxy dominated" cluster, which means that the diffuse X-ray emission from the cluster is strongly dominated by emission from the central giant elliptical galaxy M87. The size of the X-ray core of M87 is much smaller than the size of X-ray core of Coma cluster, so that in spite of the fact that Virgo is about 5 times closer to the Earth than Coma, the angular size of its core, $r_0 \simeq 2$ arcmin, is 5 times

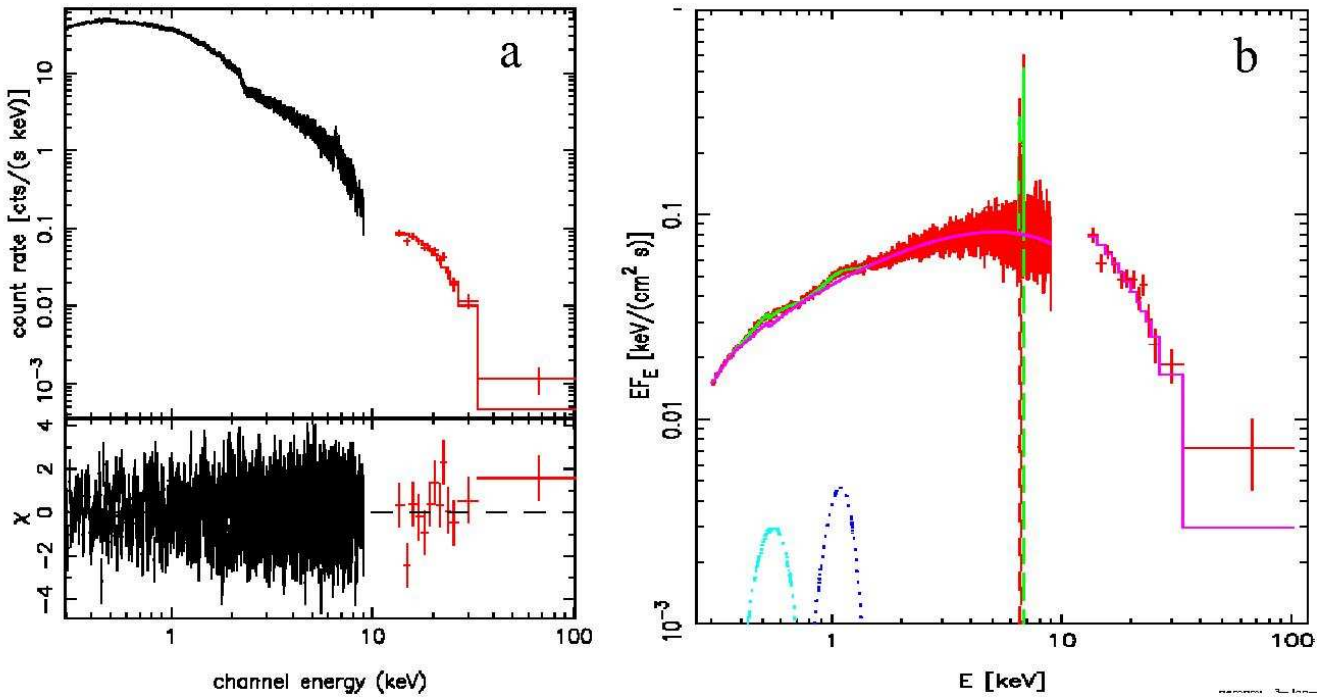

Figure A1. Folded (a) and unfolded (b) XMM-Newton and Beppo-SAX spectrum of the Coma galaxy cluster. The simple phenomenological model used to fit the data consists of a cutoff powerlaw modified by the galactic absorption and four Gaussian lines. The model parameter values are given in the text.

less than the one for Coma. This, in turn, implies that the temperature of the intracluster (or intragalactic) medium varies significantly over the XMM FoV, which extends up to $6-7r_0$. Finally, Virgo cluster is not a relaxed galaxy cluster, and assumptions about hydrostatic equilibrium, which one has to evoque to compute the DM distribution may not hold.

The above facts make the modelling of the X-ray spectrum collected from the entire XMM FoV difficult. However, we achieve a satisfactory phenomenological fit the the Virgo cluster spectrum with the model similar to the one used in the previous Section for Coma cluster analysis. It consists of the powerlaw with the photon index $\Gamma = 1.28$ modified at high energies by an exponential cut-off at $E_0 = 2.22$ keV and at low energies by photoelectric absorption on the Galactic hydrogen column density $N_H = 2.5 \times 10^{20}\,\mathrm{cm}^{-2}$. Several lines have to be added to the fit, to make it acceptable. In particular, Fe Kα and Kβ lines of Fe (6.7 and 7.9 keV), line of O at 0.64 keV, a set of lines at 1 keV from the cooling flow in the center of Virgo cluster, etc. (7 lines altogether).

APPENDIX C: SIMPLE MODEL FOR THE X-RAY SPECTRUM OF THE RING WITH THE RADIUS $9' - 11'$ AROUND M87.

We repeat the procedure already used for the analysis of the central parts of Coma and Virgo clusters for the present case. Namely, we find a simple phenomenological fit to the broad-band spectrum which in this case is given by the cutoff powerlaw with $\Gamma = 1.29$ and $E_0 = 2.24$, modified by the Galactic absorption. Again, we add several lines (as in the case of the previous Appendix) to make fit acceptable.

REFERENCES

Abazajian K., 2005, ArXiv e-print astro-ph/0511630

Abazajian K., Fuller G. M., Tucker W. H., 2001, ApJ, 562, 593

Ahmad Q. R., et al., 2002, Phys. Rev. Lett., 89, 011301

Arnaud M., Evrard A. E., 1999, MNRAS, 305, 631

Barger V. D., Phillips R. J. N., Sarkar S., 1995, Phys. Lett., B352, 365; Erratum-ibid. B356, 617

Boehringer H., Belsole E., Kennea J., Matsushita K., Molendi S., Worrall D. M., Mushotzky R. F., Ehle M., Guainazzi M., Sakelliou I., Stewart G., Vestrand W. T., Dos Santos S., 2001, A&A, 365, L181

Boyarsky A., Neronov A., Ruchayskiy O., Shaposhnikov M., 2005, ArXiv e-print astro-ph/0512509

Briel U. G., et al., 2001, A&A, 365, L60

Briel U. G., Henry J. P., Boehringer H., 1992, A&A, 259, L31

Cavaliere A., Fusco-Femiano R., 1976, A&A, 49, 137

Dodelson S., Widrow L. M., 1994, Phys. Rev. Lett., 72, 17

Dolgov A. D., Hansen S. H., 2002, Astropart. Phys., 16, 339

Eguchi K., et al., 2003, Phys. Rev. Lett., 90, 021802

Evrard A. E., Metzler C. A., Navarro J. F., 1996, ApJ, 469, 494

Fabricant D., Gorenstein P., 1983, ApJ, 267, 535

Fukuda Y., et al., 1998, Phys. Rev. Lett., 81, 1562

Gruber D. E., Matteson J. L., Peterson L. E., Jung G. V., 1999, ApJ, 520, 124

Liedahl D. A., Osterheld A. L., Goldstein W. H., 1995, ApJ, 438, L115

McLaughlin D. E., 1999, ApJ, 512, L9

Mewe R., Lemen J. R., van den Oord G. H. J., 1986, A&AS,

65, 511
Neumann D. M., Lumb D. H., Pratt G. W., Briel U. G., 2003, A&A, 400, 811
Nulsen P. E. J., Bohringer H., 1995, MNRAS, 274, 1093
Pal P. B., Wolfenstein L., 1982, Phys. Rev., D25, 766
Raymond J. C., Smith B. W., 1977, ApJS, 35, 419
Sarazin C. L., Bahcall J. N., 1977, ApJS, 34, 451
Schindler S., Binggeli B., Böhringer H., 1999, A&A, 343, 420
Strumia A., Vissani F., 2005, Nucl. Phys., B726, 294
Young A. J., Wilson A. S., Mundell C. G., 2002, ApJ, 579, 560